Constraining the Early History of Mercury and Its Core Dynamo by Studying the Crustal Magnetic Field

Joana Oliveira, Lon Hood, Benoît Langlais

Constraining the Early History of Mercury and its Core Dynamo by Studying the Crustal Magnetic Field

Joana S. Oliveira[1,2], Lon L. Hood[3], Benoit Langlais[4]

[1]ESA/ESTEC, SCI-S, Keplerlaan 1, 2200 AG Noordwijk, Netherlands

[2]CITEUC, Geophysical and Astronomical Observatory, University of Coimbra, Coimbra, Portugal

[3]Lunar and Planetary Laboratory, 1629 E. University Blvd., Univ. of Arizona, Tucson, AZ 85721, USA

[4]Laboratoire de Planétologie et Géodynamique, Université de Nantes, Université d'Angers, CNRS, UMR 6112, Nantes, France

Key Points:

- We analyze crustal magnetic anomalies that are likely thermoremanent and obtain the corresponding paleopole positions.
- All best fitting paleopoles are found in the Southern Hemisphere.
- Our study strongly suggests that Mercury has evolved with time.

This article has been accepted for publication and undergone full peer review but has not been through the copyediting, typesetting, pagination and proofreading process which may lead to differences between this version and the Version of Record. Please cite this article as doi: 10.1029/2019JE005938

Corresponding author: Joana S. Oliveira, Joana.Oliveira@esa.int

Abstract

Low altitude magnetic field data acquired by MESSENGER over a small portion of Mercury's surface revealed weak crustal magnetic field signatures. Here we study the crustal magnetic anomalies associated with impact craters on Mercury. We assume that the sources of these anomalies consist of impact melt, enriched in impactor iron. We assume that the subsurfaces of Mercury's impact craters have cooled in the presence of a constant global magnetic field, thus becoming thermoremanently magnetized. We invert for the crustal magnetization direction within five craters using a unidirectional magnetization model which assumes that the melt impact rocks recorded the constant core magnetic field present when the crater was formed, and that the crater's magnetization has not been altered since its formation. From the best fitting magnetization direction we then obtain the corresponding north magnetic paleopole position assuming a centered core dipolar field. Results show that all five magnetic paleopoles lie in the Southern Hemisphere but are not required to be located near the present-day magnetic pole, which lies near the south geographic pole. Accounting for the uncertainties, we show that our results all agree in a common small region that excludes the current magnetic pole. This strongly suggests that the dynamo has evolved with time. Our results represent valuable information for understanding the evolution of Mercury, and emphasize the importance of including more anomaly analyses to complete and refine our conclusions.

1 Introduction

The MESSENGER spacecraft orbited Mercury during roughly 4 terrestrial years acquiring important information on the internal magnetic field of Mercury. Recent studies have shown that the core magnetic field of Mercury is dipolar with a strong quadrupolar component (Anderson et al., 2012; Oliveira et al., 2015; Thébault et al., 2018). The lack of small scales is an astonishing observation (Oliveira et al., 2015; Thébault et al., 2018), and is very difficult to be explained by dynamo models. Several numerical dynamo simulations have tried to explain such observations but mostly fail to produce all observed characteristics. Those models include dynamos operating in a thin shell (Stanley et al., 2005; Takahashi & Matsushima, 2006), a strong dynamo with a stably-stratified layer in the top of the core (Christensen, 2006; Christensen & Wicht, 2008), snow iron processes in the core (Vilim et al., 2010), or even a heterogeneous heat flux pattern at the core-mantle boundary (CMB) (Cao et al., 2014). However, using specific dynamo pa-

rameters, most of the models explain at least some of the characteristics of the observed field. Recently, numerical simulations combining double-diffusive convection with a stably stratified layer reproduced the present magnetic field of Mercury (Takahashi et al., 2019) showing that the equatorial asymmetry could last for millions of years. More importantly, to date, none of those models use observational constraints for the early stages of the dynamo.

Only during its low altitude campaign MESSENGER acquired important information on the crustal magnetic field of Mercury. However, the small magnetosphere of the planet (Johnson et al., 2012; Anderson et al., 2012), the strong field variability due to external sources (Korth et al., 2012), and the relatively weak crustal fields (Purucker et al., 2009; Hood, 2015, 2016; Hood et al., 2018; Johnson et al., 2015) combined with the very eccentric spacecraft orbit represent obstacles for investigating the nature of the crustal field. Indeed, available crustal magnetic field maps only span a small portion of the Hermean surface, between 35° and 75° North over all longitudes. Crustal magnetic field maps reveal anomalies heterogeneously distributed within the (mapped) surface. The strongest intensities at 40 km altitude of, ~ 10 nT, are found within the Caloris basin. Many of the anomalies are not found to correlate either with the topography, surface geology, or gravity (Hood, 2016; Hood et al., 2018). Some important exceptions are found for anomalies within some craters (e.g., Rustaveli and Vyasa) and basins (e.g., Caloris), however (Hood, 2016; Hood et al., 2018).

The exact nature of crustal magnetic field sources is difficult to determine when using solely spacecraft measurements. The sources generating the observed crustal fields could, in principle, be either ancient remanent magnetization or merely induced magnetization (IM) caused by permeability contrasts in the presence of Mercury's existing core dynamo field. Ancient remanent magnetism could be caused by different processes such as shock remanent magnetization (SRM) and thermoremanent magnetization (TRM). TRM and IM would record the ancient or the present core field direction, respectively. The early history of planets can be assessed by studying the crustal magnetism, only when the sources are remanently magnetized. Many crustal field studies for the Earth, Mars, and the Moon have allowed constraints to be placed on the early history of those bodies. For instance, on Earth, studies on the Atlantic Ridge crustal fields revealed that the terrestrial dynamo has undergone many resersals of polarity (Vine & Matthews, 1963). For Mars and Moon, true polar wander (TPW) events, dynamo polarity reversals, a dif-

ferent morphology dynamo field, and, in the lunar case, evidence for iron-rich impactors, have been inferred (Arkani-Hamed, 2001; Takahashi et al., 2014; Wieczorek et al., 2012).

Contrary to these bodies, Mercury, like the Earth, possesses a core magnetic field. The major difficulty when studying the crustal magnetic field of such a body is to distinguish how the sources are magnetized. In this respect, calculations concerning the dependency of Curie temperature on depth have shown that at least part of the crustal field of Mercury is generated by TRM sources (Johnson et al., 2015; Hood et al., 2018). In the other hand, as for the lunar case (Wieczorek et al., 2012), it was suggested that impactor-delivered iron could be the main source material of crater-associated magnetic anomalies on Mercury. If the main source material of the Hermean crater-associated anomalies is impactor iron, then the IM source signal is too weak to explain the observed anomaly amplitudes (Hood et al., 2018) . Therefore, the anomalies associated with craters are the best option to choose if one wishes to study the ancient magnetic field.

On Earth, the majority of impact molten rocks contain remains of the projectiles, with projectile abundances in the melt sheet reaching several percent in weight (Tagle & Hecht, 2006; Tagle et al., 2009). We assume that this could also be the case for Mercury, as was also sugested by Hood et al. (2018). The Hermean surface is generally metal iron poor (Weider et al., 2014), and the magnetic anomalies could be a result of impactor-metal iron that was carried to the surface of Mercury. Anomalies within the center of relatively fresh complex impact craters are the most appropriate for paleopole studies. Complex impact craters are large enough to contain a melt sheet with the thickest region in its center (e.g.,Cintala and Grieve (1998)). This melt sheet would have cooled slowly with time scales of about a million year. Compared to long-lived core dynamo time scales, crater melt sheets cool fast enough to record thermoremanently a constant and unidirectional surface field. In addition, studying anomalies associated with fresh craters reduces the probability of potential demagnetization processes, such as other impacts, unstable terrain near the crater boundaries and, space weathering. On the other hand, considering that the crust was previously magnetized, the vertical extent of the crater center corresponds to the region that suffers high levels of shock and pressure demagnetization. It was observed in laboratory experiments, under certain conditions, that the demagnetization of the rocks can reach levels above 50% (Gattacceca et al., 2010; Bezaeva et al., 2010).

Crater-associated anomalies on Mercury can be used to estimate the direction of magnetization. If these anomalies are of TRM origin, converting the magnetization direction to paleomagnetic pole positions, would give valuable insights. The present day Mercury core dynamo field has its magnetic north pole located near the geographic south pole (e.g., Anderson et al. (2012)). Therefore, if the paleopoles are not found close to the geographical poles, true polar wander events or a different magnetic field morphology could explain such results. Alternatively, if some paleopoles are found in the Northern Hemisphere, this would suggest not only that the dynamo underwent polarity reversals but also proves that the sources are unequivocally TRM in origin. In all cases, this would be indicative that the ancient dynamo field was different from that of nowadays.

Small and isolated crustal magnetic field anomalies on Mercury can be used to infer the magnetization direction based on the unidirectional assumption. Here we invert for the direction of crustal magnetization associated with Hermean isolated anomalies within craters using the approach initially developed by (Parker, 1991). In this method, the only assumption made is that the magnetization direction is constant within the analyzed region of the crust. The strength of this method is that it makes no assumptions about the source geometry. Recently, this approach has been applied to planetary magnetic crustal fields to determine paleopole locations for the Moon (Oliveira & Wieczorek, 2017) and Mars (Thomas et al., 2018). Another slightly different application has combined the unidirectional model with laboratory thermoremanent experiments to determine iron abundances within basins on the Moon (Oliveira et al., 2017).

In this work, we make use of a global crustal magnetic field model based on MESSENGER low altitude campaign measurements (Hood, 2016; Hood et al., 2018) and apply the technique of (Parker, 1991) to the Hermean isolated magnetic anomalies associated with craters. In section 2, we describe the methodology of inverting crustal magnetic field data for a unidirectional magnetization distribution (Parker, 1991) and how it is applied to Mercury. Next, in section 3 we show the results for all the anomalies associated with craters. In section 4, different hypotheses that could account for our derived distribution of paleopoles are discussed. Finally, we make our concluding remarks on how our results might help to place constraints on the Hermean evolution models.

2 Method

In order to determine new constraints on the early history of Mercury we investigate isolated magnetic anomalies associated with impact craters. We use the method of Parker (Parker, 1991) which was first applied to estimate the magnetization direction of terrestrial seamounts. This method assumes a unidirectional magnetization volume source model, consistent with the hypothesis of a melt sheet cooling down in a stable global ambient field. For a melt sheet occupying the interior of a large basin such as Caloris, this might not be a valid assumption because: 1) different areas and/or different depths of the basin may have cooled at different rates and the core dynamo field may have changed between one TRM acquisition event and another; 2) the direction of the core dynamo field is changing over the surface of the planet. For instance, (Parker, 1991) showed that when inverting for the magnetization direction of synthetic samples with mixed polarity magnetizations, the method did not retrieve a single solution. However, for single anomalies within craters, such as those to be considered here, it is reasonable to assume that the melt sheet cooled uniformly in a constant dynamo field. As shown by (Parker, 1991), a volume (i.e., continuous distribution) of unidirectional magnetization is mathematically equivalent to discretized unidirectional dipoles placed at the volume's boundary (i.e., its top surface), reducing significantly the dimensionality of the problem. The magnetic moments of the unidirectional dipoles distribution are allowed to vary with position, and therefore the magnetization is described as,

$$\mathbf{M}(\mathbf{s}_i) = \hat{\mathbf{m}}\, m(\mathbf{s}_i), \qquad m(\mathbf{s}_i) \geq 0 \tag{1}$$

where $\hat{\mathbf{m}}$ is the unit vector of magnetization $\mathbf{M}$, and $m(\mathbf{s}_i)$ is the dipole moment at vectorial position $\mathbf{s}_i$. Note that we arbitrarily impose positive dipoles instead of negative ones.

In his initial study, Parker (1991) analyzed the field component that is aligned with the global field. Lunar and martian studies that used the same method analyzed a single component because none of those bodies contain a present global field. In the case of Mercury, though a global field is present, we choose to follow the lunar and martian studies using the radial component. The magnetic field d in the radial direction $\hat{r}$ at observation point j is calculated as the sum of the contributions from the dipoles located

at positions $\mathbf{s}_i$

$$d_j = \sum_{i=1}^{N_d} g_j(\mathbf{s}_i)\, m(\mathbf{s}_i), \qquad j = 1, ..., N_{obs} \tag{2}$$

where the contribution of a single dipole at location i is given by

$$g_j(s_i) = \frac{\mu_0}{4\pi} \left(\frac{3\hat{\mathbf{m}} \cdot (\mathbf{r}_j - \mathbf{s}_i)\, \hat{\mathbf{r}}_j \cdot (\mathbf{r}_j - \mathbf{s}_i)}{|\mathbf{r}_j - \mathbf{s}_i|^5} - \frac{\hat{\mathbf{m}} \cdot \hat{\mathbf{r}}_j}{|\mathbf{r}_j - \mathbf{s}_i|^3} \right). \tag{3}$$

N_{obs} and N_d correspond to the number of observations and the number of dipoles at the surface, and $\mathbf{r}_j$ and $\mathbf{s}_i$ are the vector positions of the observations and dipoles relative to a fixed planetocentric origin, respectively. The equations 2 and 3 may be combined into a matrix form as

$$\mathbf{d} = \mathbf{G}(\hat{\mathbf{m}})\, \mathbf{m}, \tag{4}$$

where $\mathbf{d}$ is a vector of the magnetic field observations projected in the radial direction, the matrix $\mathbf{G}$ depends upon the assumed direction of magnetization $\hat{\mathbf{m}}$ and contains the elements given by eq. 3, and $\mathbf{m}$ is a vector that contains the dipole moments of the surface dipoles at locations $\mathbf{s}_i$. All dipole moments are taken to be positive.

Following Parker (1991), with the elements of vector $\mathbf{m}$ positive we use the technique of nonnegative least squares analysis developed by (Lawson & Hanson, 1974) to solve equation 4. One of the advantages of this technique is that only a maximum of N_{obs} out of N_d dipoles are needed to explain the magnetic field observations. Therefore, using a number of N_d surface dipoles larger than the number of observations (N_{obs}), allows the nonnegative least squares (nnls) technique to determine automatically which dipoles have nonzero values.

In pratice, we follow the same modelling procedures as those used by (Oliveira & Wieczorek, 2017) and (Oliveira et al., 2017) in lunar studies. First, a grid of homogeneously distributed dipoles (Katanforoush & Shahshahani, 2003) of 0.4° resolution is placed in the planet's surface within a circle of radius r_d around the crater center. Here we fix r_d to be equal to the crater rim radius, as TRM sources (i.e., the crater melt sheet) are supposed to lie within this boundary. The magnetic field data used in the inversion scheme are contained within a circle of radius r_{obs} that is 1° larger than the dipoles circle radius, r_d. As shown by (Oliveira & Wieczorek, 2017) this difference in the circles radii avoids strong edge effects of the modeled field. Taking into account the nnls property mentioned above, we choose the initial number of dipoles (N_d) to be much larger than N_{obs}, allowing the technique to determine the dipoles that are positive.

For each magnetization direction $\hat{\mathbf{m}}$ we perform the inversion to determine the dipoles position, their dipole moments, and the RMS misfit between the observations and modelled magnetic field. We vary the magnetization direction over all directions in a unit sphere. Each vector is centered in a unit sphere pointing to each surface point spaced of 4° over an equidistant spherical grid (Katanforoush & Shahshahani, 2003). Each magnetization direction is converted to the corresponding magnetic north paleopole position, as explained by Butler (1992). We then plot a map of the RMS misfit as a function of the paleopole position. The lowest RMS misfit value of the map corresponds to the best fitting paleopole position.

We note that the instrument uncertainty and the Equivalent Source Dipoles (ESD) model formal uncertainties are too small to give a reasonable uncertainty value for our inversions. In practice, we calculate the RMS difference between the observed and modelled radial field points located between the circles of radii r_d and r_{obs}, respectively. Our uncertainty is obtained by calculating the maximum allowable misfit, i.e., the upper limit of RMS values for which the corresponding solution is accepted, and is based on the assumption that the magnetic field signal surrounding the isolated anomaly should not be inconsistent with that calculated from the unidirectional model. All models with inversion uncertainties lower than the allowable misfit are therefore a possible paleopole position.

By definition, for an isolated anomaly it is not expected to observe anomaly-related signals far from the principal anomaly. If there is any signal that is inconsistent with the modeled anomaly then the uncertainty would likely be larger. On the other hand, if the signal of the surrounding area is weak, then the uncertainty is expected to be smaller. Synthetic tests based on Parker's method performed by Thomas et al. (2018), show that in the presence of a secondary anomaly in the vicinity of the principal one, a solution that includes half of the planet surface is obtained. We have extended the synthetic study using synthetic magnetized sources instead of a single dipole as previously done, to understand if our estimations could be affected. The paleopole positions were retrieved correctly independently of the source body used. Weaker secondary anomalies are often present in the vicinity of each studied crater, which could perturb our inversion results. As the Parker method is designed to invert for the magnetization direction of a single isolated anomaly, we chose to reduce the observations' area circle size, when necessary, to avoid secondary anomalies. This, in turn, affects the dipoles' grid area circle, which

will be slightly smaller than the impact crater area itself. We expect that final results would not be affected by slightly reducing the study area, however.

3 Analysis of anomalies associated with craters

In this section, we first briefly present the input model of the hermean crustal magnetic field, specifying the anomalies studied here. Next, we show the results by discussing each anomaly in detail.

3.1 Data

We use the gridded crustal magnetic field model at 40 km altitude derived by Hood (2016) and Hood et al. (2018), which uses magnetometer data from the low-altitude passes of the spacecraft during the last three months of the MESSENGER mission. This model is based on the equivalent source dipole (ESD) technique, which was applied to data previously long-wavelength and high pass filtered from non-crustal sources (e.g., internal core field and magnetosphere sources). The grid has 1° and 0.5° resolution in longitude and latitude, respectively, and only covers latitudes between 35° and 75° due to the spacecraft orbit configuration. In this study, we will make use only of the radial field component. To determine their model (Hood, 2016) and (Hood et al., 2018) made use of only the radial field measurements, as horizontal components are highly susceptible to contamination by non-crustal fields.

From our survey, we found five anomalies that are likely related to the crater forming process: Rustaveli, Vyasa, and three other unnamed craters. Note that we chose to follow the same terminology as that of Table 1 from (Hood et al., 2018) to identify the craters. Figure 1 shows the locations of the anomalies associated with craters analyzed in this study superposed with the crustal magnetic field intensity map. Note that we have access to the crustal magnetic field information over a small portion of latitudes of the planet only, due to the very eccentric MESSENGER spacecraft orbit configuration. Though important external field contamination is believed to prevail in the northern and southern boundaries of the map, the anomalies of this study are not located in their vicinity. In this section, we first describe the inversion steps for the craters in our study. We show the results for the five anomalies associated with craters. Following this, we show the global picture of the resulting paleopoles.

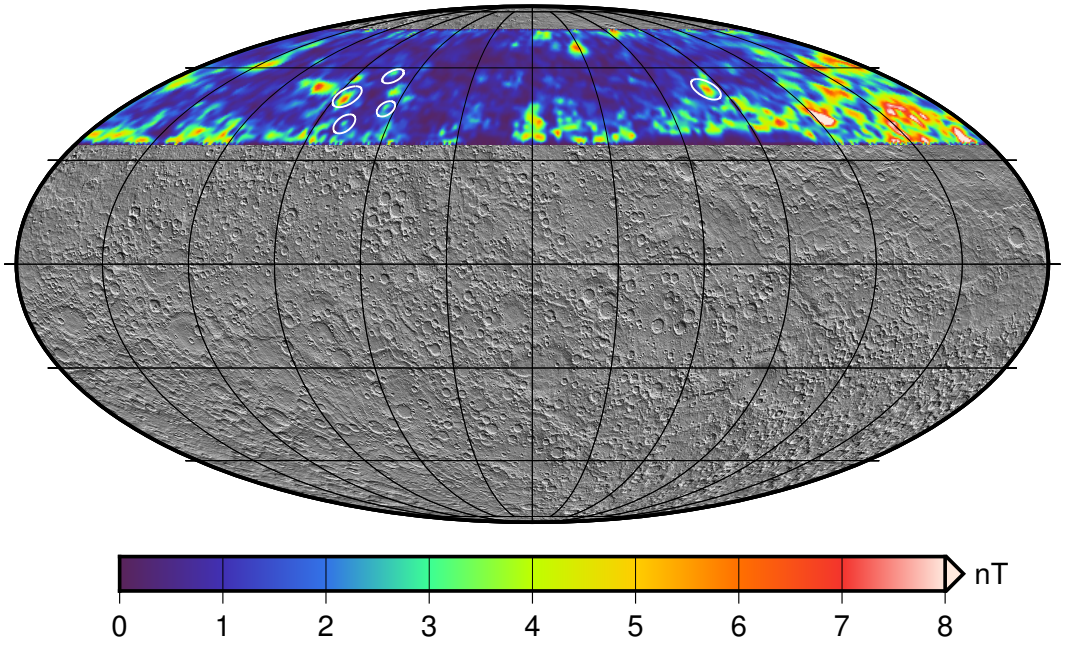

Figure 1. Crustal magnetic field strength of Mercury at 40 km altitude from (Hood, 2016; Hood et al., 2018) based on MESSENGER observations. White circles indicate the locations of the magnetic anomalies investigated in this study. Projection is global Molleweide, centered on the 0° meridian.

3.2 Results

We performed inversions for five anomalies that are associated with impact craters of diameter varying from 130 to 300 km. As mentioned above, we follow the same numbering order of craters as in (Hood et al., 2018) (See Figure 3b of that reference for a topographical map of the crater locations). Figure 2 shows, for each anomaly, the topographical map (left column), the magnetic field intensity at 40 km altitude (middle column) and, the location of the nonnegative dipoles retrieved by the inversion (right column). In all charts, we delimit the grid of observations and that of dipoles used in our inversions by a solid and dashed black circles of radii r_{obs} and r_d, respectively. For the sake of completeness, we show in the supporting information the radial magnetic field data component, the best fitting radial magnetic field (i.e., the modelled field), and the difference between the two. In addition to the circles we also plot the locations of the observations and the dipoles used in the inversion. Finally, Figure 3 shows how the misfit varies with the north magnetic pole position, where the star symbol denotes the best fitting solution and the white line corresponds to the uncertainty.

Table 1. Location (Lon, Lat), radii of observations (r_{obs}) and dipoles (r_d), number of observations (N_{obs}) and dipoles (N_d) used in the inversion, the number of non-zero dipoles (Nz_d) of the best-fitting calculated model, North paleopole position (ϕ_p, θ_p), the RMS misfit between the best-fitting model and the data, and the corresponding uncertainty.

#	Name	Lon (°)	Lat (°)	r_{obs} (°)	r_d (°)	N_{obs}	N_d	Nz_d	ϕ_p (°)	θ_p (°)	Misfit (nT)	σ (nT)
1	Rustaveli	82.5	52.5	3.5	2.5	128	148	43	66.8	-62.6	0.715	1.195
2	Vyasa	275.0	50.0	3.5	2.5	110	155	44	246.8	-50.9	0.442	0.795
3	-	289.0	57.0	3.0	2.0	104	96	14	289.0	-2.2	0.487	0.780
4	-	295.2	46.8	2.0	1.0	37	27	5	240.9	-34.8	0.588	0.837
5	-	281.8	41.2	2.5	1.5	50	56	12	29.6	-50.6	0.324	0.594

In Table 1 we provide detailed information for each anomaly, including the center location (longitude and latitude) of the crater that is associated with the magnetic anomaly, the radius of the observations circle, r_{obs}, and that of the dipoles, r_d, the number of observations, N_{obs} and the number of dipoles, N_d, the nonzero dipoles retained by the inversion Nz_d, the north paleomagnetic pole position (ϕ_p , θ_p), the RMS misfit, and the uncertainty value, σ.

3.2.1 Rustaveli

Rustaveli, (82.5°E, 52.5°N), is a crater of medium size with an approximate diameter of 200 km located in a relatively flat region with few small craters in its vicinity. Rustaveli is a good example of a magnetic anomaly correlated with an impact crater, not only because of its relatively strong field but also because it is an impact crater with relatively unaltered topography. Comparing the magnetic field signal with the topography of the crater we see that almost all of the magnetic anomaly is within the crater main rim. Though the strongest signal of the anomaly is confined to the crater rim, the entire anomaly is somewhat elongated toward the northeast of the crater or is not completely dissociated from a much weaker secondary anomaly outside the crater's main rim. We chose not to model this secondary anomaly because it is not located in the crater's melt sheet and therefore has undefined sources origin.

Our method retrieves well the radial magnetic field with an RMS misfit of 0.72 nT, which is much lower than the central anomaly strength ($\sim$ 6 nT). First, we observe that only few dipoles are retained to explain the radial field. Secondly, comparing the distribution of dipole moments with the magnetic field observations, we note that the strong dipoles are slightly offset towards the north when compared to the magnetic field strength's

peak. If the positions of the nonnegative dipoles are indicative of the sources' position, then the asymmetric nonnegative dipoles distribution might be explained by the process of a projectile that impacted the surface at an oblique angle, as shown in lunar simulations by (Wieczorek et al., 2012).

The best fitting magnetization direction is pointing down towards the planet's surface (inclination 44° and declination 8°) resulting in a north magnetic paleopole position at (66.8°E, 62.6°S). We note that for a core field predominantly generated by a central inducing dipole aligned with the rotation axis, the paleopole position is located at the geographic poles. Additionally, extrapolating the model of the present core magnetic field to the Southern Hemisphere, it is expected to find the magnetic north pole to be located at the geographic south pole. This is roughly 30° apart from our best fitting paleopole result. The calculated uncertainty of 1.2 nT is larger than the best fitting RMS misfit value of 0.72 nT. This results in having the entire Southern Hemisphere of the planet as a possible solution for the location of the palaeopole.

3.2.2 Vyasa

Vyasa, centered at (275°E, 50°N), is our preferred case due to its high magnetic peak strength of roughly 7 nT. The anomaly peak is found within the crater rim but is displaced slightly to the south of its center. The magnetic anomaly is somewhat elongated towards the southern direction, slightly crossing the crater rim. Vyasa impact crater, with a diameter of approximately 300 km, has its rim degraded by two other smaller secondary anomalies on the northeast and northwest sides. Additionally, we observe a weaker magnetic anomaly associated with the northwest secondary crater.

Our method explains well the radial magnetic field with an RMS misfit of 0.44 nT, again much lower than the peak strength of ∼7 nT. The magnetization vectors have an inclination of 26° and declination of 18°. The model, as for Rustaveli, needs few dipoles to explain the magnetic anomaly. The strongest retained dipoles are roughly distributed in the center of the impact crater and are not shifted towards the south as happens with the observed magnetic anomaly itself. The best fitting paleopole position is at (247°E, 51°S) which is farther from the geographic south pole than in the previous case. Taking into account the uncertainty value, it is possible that the paleopole could be anywhere south of 30°S. Overall results, Vyasa has the best constrained paleopole position con-

sistent with the fact that its magnetic anomaly is the strongest among the five anomalies of this study. In addition, we also performed an inversion of the small anomaly related to the secondary crater located northwest of Vyasa. Its best fitting paleopole position is located at (275°E, 49°S) with an RMS misfit of 0.42 nT, which is only 18° from the Vyasa paleopole.

3.2.3 Anomaly 3

The anomaly 3 is correlated with a unnamed impact crater centered at (289°E, 57°N), with an approximate diameter of 136 km. We note that the impact crater is located in the vicinity of some elevated terrains associated with younger craters. The magnetic anomaly is shifted towards the north of the crater's center, and it shows a weak elongated signal which falls slightly outside of the crater rim in the same direction.

We model the radial component of anomaly 3 with an RMS misfit of 0.49 nT, which is low comparing to the anomaly peak strength of 3.5 nT. The magnetization vectors have an inclination of -50° and declination of 18°. Only 14 out of 96 dipoles within the crater rim are needed to describe the anomaly. The dipoles do not show any particular preference in their distribution, but the strongest dipoles are lying roughly where the magnetic anomaly is. The best fitting paleopole position is found near the geographic equator at (289°E, 2°S), corresponding to a distance of about 90° from the geographic poles. In addition, accounting for the uncertainties, contrary to the other cases, the geographic south pole is excluded from the solution. Instead, the geographic north pole is a possible solution for this case.

3.2.4 Anomaly 4

The anomaly 4 is related to the impact crater centered at (295°E, 47°N). The peak of the anomaly is shifted east of the center of the crater. This anomaly presents several differences in respect to the other cases, such as: 1) the crater morphology is more complex, showing several overlapping younger craters; 2) the crater size is the smallest of all the cases considered in this study; and 3) we use an area of observations smaller than the crater size to avoid a relatively strong and large magnetic anomaly, which appears to be related to the elevated terrain south-east of the crater.

The magnetic radial field is explained with an RMS misfit of 0.59 nT, smaller than the peak strength of ∼3.5 nT. The magnetization vector has an inclination of 10° and declination of 42°. Only 5 out of 27 available dipoles are necessary to explain the observed field. The nonnegative dipoles are placed east of the crater center, where the anomaly peak is found. The best fitting paleopole position obtained is located at (241°E, 35°S). Not surprisingly, accounting for the uncertainty, more than half of the planet might contain the possible paleopole solution. Although this result is not robust, it was expected due to the limitations that this particular anomaly faces. However, similar to all the other cases except the anomaly 3, it contains the geographic south pole as a possible solution for the paleopole position.

3.2.5 Anomaly 5

The anomaly 5 is related to the unnamed impact crater centered at (282°E, 41°N), corresponding to our southernmost case. The position of the crater is sufficiently far from the map limit so that the signal is not perturbed by edge effects. The impact crater morphology is perturbed by two other smaller impact craters southwest and south of the crater's center. However, none of those smaller craters seem to perturb the isolated magnetic anomaly signal. In addition, the magnetic field anomaly is relatively small, and it is roughly centered on the impact crater.

The radial field component is explained with an RMS misfit of 0.3 nT, which is much weaker than the peak strength of ∼3.5 nT. The magnetization vectors have an inclination of -50° and declination of 30°. Only 12 dipoles from 56 available dipoles are used to describe the magnetic anomaly. The nonnegative dipoles are mainly distributed where the magnetic anomaly is, which is the case for the anomalies 3 and 4. The best fitting paleopole position obtained is located at (30°E, 51°S). This corresponds to a distance of 40° from the geographic south pole, similar to the paleopole position found for Vyasa anomaly. Accounting for the uncertainty, a large part of the Southern Hemisphere could be a possible solution, similar to the Rustaveli case.

4 Discussion: Constraining the early history of Mercury

In this section, we first discuss the distribution of the paleopoles obtained for all the studied anomalies. Then, we consider the possibility that the anomaly sources might

be magnetized by induction in the present-day Mercury field. Finally, assuming that our sources carry thermoremanent magnetization, we consider and discuss separately two different main hypotheses that can explain our paleopoles distribution: True polar wander process and ancient dynamo field morphology. Through out all section we discuss our results with three different perspectives: 1) our paleopoles within uncertainties which is a conservative approach but, is our preferred one as uncertainties should be associated to any result; 2) that our uncertainties are calculated in a conservative way, and therefore we focus on paleopoles best fitting position for discussion purposes; and 3) that all our craters were formed during the same conditions field, and therefore we focus on the overlapping of results.

4.1 Paleopoles distribution

Figure 4 shows the distribution of the best-fit north magnetic paleopoles together with the corresponding uncertainties for all studied anomalies. We find the best fitting paleopoles at latitudes between 2°S and 62°S. The associated uncertainties are large, and cover approximately one hemisphere in most cases. Despite the individual large uncertainties, all paleopole solutions overlap in a relatively small common region. This common region is located between 30°S and 80°S latitudes, and between 170°E and 300°E longitudes. This region could be perceived as the most probable solution, if we assume that our five craters formed with an Hermean magnetic field of similar morphology. We emphasize that the southernmost latitude of this overlapping region is only 10° away from the geographic south pole. Rather small angular distances between this possible paleopole position and the geographical south pole can be explained by true polar wander events (see subsection 4.3).

Although our sample size is small with only five studied anomalies, they can nonetheless be discussed as they offer consistent results. Four of the five anomalies results suggest that the paleopoles are located in the Southern Hemisphere. In addition, another interesting feature that we can observe is that the best fitting paleopoles do not seem to be randomly distributed across the Hermean surface, with the entire Northern Hemisphere showing a lack of magnetic best fitting paleopoles. Additionally, none are found in the immediate vicinity of the geographic poles as would be expected for a dipolar core field aligned with the planet's rotation axis. However, three best fitting paleopoles lie at latitudes exceeding 50°S, and can therefore be considered to be high-latitude pole po-

sitions. The anomaly 3 has its best fitting paleopole at an equatorial position, but this is also the poorest constrained result. For this particular anomaly, the geographic north pole is within the solution area. This would imply a geomagnetic north pole close to the geographic north pole, in contradiction to the other four results. This is however not unexpected, as polarity reversals are a very common feature of dynamos. Furthermore, we observe that the best fitting paleopoles for Rustaveli and anomaly 5 are very close to each other, despite the anomalies being far away. The same situation is found for both Vyasa and anomaly 4 (note that the paleopole for the secondary crater anomaly near Vyasa is also located nearby).

We conclude that our results do not exclude a reversal, but neither do they imply one. Future inversions of further anomalies of TRM origin are required to refine our conclusions. In the following, we discuss the remanent or induced origin of the modeled anomalies. Next, we discuss the different hypotheses that can explain our results, which are usually called to explain planetary evolution. In particular, we consider true polar wander events and different ancient dynamo morphology scenarios.

4.2 Anomaly source origin

As explained in the Introduction, in order to constrain the early history of Mercury's interior and axial orientation, we have to assume that our magnetic sources are related to ancient TRM rather than induced by permeability contrasts in the crust by the present-day core dynamo field. However, in practice, distinguishing IM from TRM sources is not straightforward. We also recognize that, if they exist, large-scale lithospheric field originated by deeper sources might be filtered out when constructing the magnetic field model. This in turn prevent us to access the contribution of unknown large-scale lithospheric field, and consequently preclude us from inferring correctly the magnetization direction (see (Vervelidou et al., 2017) for details). We expect, however, small effects from the large-scales deep sources to the shallow ones studied here. On the other hand, under the assumption of an axial dipolar field, the paleopole position of induced sources would lie near the magnetic north pole, corresponding to the present geographic south pole. However, the present-day core field is not purely dipolar, as it has a strong quadrupole component (Anderson et al., 2012; Oliveira et al., 2015; Thébault et al., 2018). In order to better distinguish between a TRM and IM origin, we investigate the distri-

bution of paleopoles that would be obtained if the magnetic anomalies were actually due to IM acquired in the presence of the present-day core magnetic field.

In order to estimate the distribution of paleopoles that would be obtained if all sources were associated with IM, we use an Hermean core field model updated from Oliveira et al. (2015). This model uses 16 Hermean days of MESSENGER measurements corresponding almost to all mission available data. The magnetic field is modeled from the north pole down to 5°N latitudes, i.e., the region where the measurements are available. We use this model to compute the inclination and declination (I, D) for latitudes ranging from 35 to 75°N on a regular grid. Next, we use these angle pairs as if they were related to the magnetization direction associated with a centered dipole and compute the magnetic paleopole position. Figure 5 shows the normalized probability of the paleopole distribution, where the darkest area corresponds to a maximum 40% probability. The resulting paleopoles distribution shows that the poles are located over a relatively large area, from the south pole up to 70°S, instead of a single polar location as expected for a purely dipolar field. We also note that the paleopoles are preferentially distributed in a band of latitudes between 70°S and 75°S. None of our best fitting paleopole locations (Figure 4) is compatible with this small area around the geographic south pole. Considering our uncertainties, however, we cannot rule out that our paleopole distribution is consistent with the IM hypothesis.

We conclude that, based on this study, paleopoles derived from IM sources cannot be distinguished from paleopoles corresponding to sources that have been magnetized by an ancient centered dipolar field. Such a distinction on the basis of paleopole estimates could only be possible if the paleopoles, accounting for their location uncertainties, are estimated to lie northward of 70°S. On the other hand, metal iron is the probable magnetic carrier present in Mercury's surface (Strauss et al., 2016). In addition, the abundance of metal iron present in the crater melt sheet is constrained by the crater's size. This is because the crater's structure is naturally related to the size, velocity and chemical composition of the impactor. Under the hypothesis that the metal iron was delivered by the projectile, Hood et al. (2018) found that the signal of magnetic sources related with craters were too strong to be explained only by induced fields.

4.3 True Polar Wander Hypothesis

True polar wander is a common pattern that is believed to have hapenned in terrestrial planetary bodies. This physical process consists of a reorientation of the body in order to adjust the major principal axis with the rotation axis after a perturbation of its mass distribution. This can happen due to external processes, e.g., impactors or due to internal processes. (Matsuyama et al., 2014). In this work, our best fitting paleopole positions are distributed over the southern hemisphere, albeit with large uncertainties. Four of the five best fitting paleopoles are found at mid- to high-latitudes, between 35°S and 63°S. To account for these paleopole positions by considering only planetary reorientation, a true polar wander of 27 up to 55 degrees is required. If we wish to explain the anomaly 3 best fitting paleopole only by means of reorientation processes, then a true polar wander of nearly 90° would be necessary.

Considering the large impact basins and highlands formation, (Keane & Matsuyama, 2018) computed a true polar wander of roughly 20°. In particular, according to their model, Caloris and Sobkou basins together with the volcanic rise can already explain a polar wander of 5 to 10 degrees. We note that 10° corresponds to the lower bound of latitudes of our common solutions region. Under the hypothesis that all craters were formed when the core field morphology was similar, TPW process could easily explain the results. If we give a particular attention to the best fitting paleopole positions, we observe that Rustaveli best fitting paleopole is located only 7° from the maximum latitude value that true polar wander events can explain. However, the reorientation directions of 120°E up to 180°E from the models of (Keane & Matsuyama, 2018) do not agree with the paleopole position longitudes of 247°E. Another case hard to be explained by TPW is the equatorial paleopole. If it is due to reorientation process only, then other geological features must be considered. For instance, the translating inner core process might also play a role in the reorientation of Mercury (Abrahams et al., 2016). Accounting for the uncertainties, all our solutions indicate that the paleopoles could be located in the actual geographic south or north poles. We emphasize, however, that our uncertainties are probably calculated in a very conservative way. Therefore, we conclude that true polar wander events are not necessary to explain our results, if we consider that the dynamo was reversing.

4.4 Ancient Dynamo Field

In general, dynamo simulations usually show several possible scenarios of dynamo evolution, which depend on the chosen parameters and the initial conditions. To account for all scenarios we discuss the degree of compatibility of our methodological approach and of our results with the three main core magnetic field morphologies that could be present at the surface during the craters formation period: multipolar field; dipolar field; and, dipolar-quadrupolar field (e.g., morphology similar to the current stage).

Although a multi-polar field hypothesis gives rise to the question of how the dynamo evolved to its current axisymmetric state, there are arguments supporting such a configuration for an ancient core field. On Mercury, Hauck II et al. (2013) infer a shallow core mantle boundary at depths of solely 420 km. Though higher multipole components decay rapidly with distance compared to the dipole component, the planetary surface being close to the core eventually favors a multipolar component field case. In this work, we used the Parker's method which inverts for the magnetization direction through an unidirectional assumption. This is still valid for an ancient multipolar field case, because 1) those component scales are much larger than the crater sizes and 2) the magnetic field is supposed to evolve on longer time scales than the time the craters molten material takes to cool down to the Curie temperature within the crater rim. However, to convert the inverted magnetization direction to its corresponding paleopole position, we make a centered dipolar field assumption. This is in contradiction with the multipolar field hypothesis. The resulting paleopoles positions would not be clustering in a small region as shown in Figure 5 (see also Oliveira and Wieczorek (2017) for another example). Our paleopole solutions indicate that an ancient multi-polar core field may have existed.

Assuming that the ancient field morphology was dipolar, then the assumption made to convert from the magnetization direction to the corresponding paleopole position is valid. It is also known from numerical simulations and from paleomagnetic records that the dynamo might undergo polarity reversals. The reversal process is thought to be much faster than the period of time that the dynamo is stable, in particular with a dominating dipolar component. During the reversal process the field morphology is thought to be dominated by the nondipolar terms. Specifically, for the Earth, the dynamo-generated field spends most of its time in a single polarity and reverses in a short period of time

compared to the time it spends in the dipolar morphology. For a crater formed during a dynamo reversal, the resulting recorded paleopole would be an average of the many directions that the field would locally take during the reversal process. For example, the time scale for a lunar melt sheet to cool down under Curie temperature is roughly 10 millions of years for 1 km thick layer (Le Bars et al., 2011). This is, however, unlikely to have happened for all craters, assuming that the dynamo spends most of its time in a dipolar configuration. The best fitting palaeolopes obtained do not cluster near the geographic poles, as expected for a reversal dynamo of centered axial dipolar morphology, nor in a small region as expected for the non-axial centered dipolar field. Accounting for uncertainties, we find a common area for all magnetic anomalies. If we assume that the Hermean magnetic field kept its morphology during our craters formation, this region could be explained by a centered non-axial dipolar field, or by an axial dipolar field present before the planet suffers a true polar wander. Our results are not in disagreement with a reversing dynamo of axial dipolar morphology as the southern/northern poles are included in the solutions.

Recently, numerical simulations combining double-diffusive convection with a stably stratified layer reproduced the present magnetic field of Mercury (Takahashi et al., 2019). This particular dynamo configuration reproduces a very stable magnetic equator offset for some magnetic diffusion times (around 60.000 years). Even if exotic, it is possible that the Hermean dynamo is extremely stable with an almost frozen surface field configuration since the craters formation period. Note that temporal variations were not found when comparing observations of Mariner 10 and those of MESSENGER (Philpott et al. 2014). In this case, the ancient field would be of the same configuration as the current one. This would lead to the magnetization distribution of the crustal magnetic field sources being the same as in the case of an IM origin, discussed in section 4.2. Consequently, the paleopoles would be found in the small region around the geographic pole as shown in Figure 5. However, our best fitting paleopoles are not found in the region where the paleopoles would lie for a field with dipolar and quadrupolar components (shown in Figure 5). Nevertheless, as shown by Takahashi et al. (2019), the evolution of the dipolar and quadrupolar terms could vary in a way that maintains the equatorial asymmetry of the field, while changing (by increasing or decreasing) the extent of the region where the paleopoles would lie. Accounting for the uncertainties, all anomalies correspond to an area of admissible paleopoles that overlaps partially or entirely with the region of pale-

poles that corresponds to today's field, preventing us from excluding this scenario. Though this work shows that the dynamo can preserve the same configuration for a few million years, a study with a longer time period is needed to confirm whether the core field morphology is stable since the crater formation period.

The exact ancient dynamo morphology is still an open question according to our paleopoles within uncertainties results. The best we can conclude from our findings is that: if the ancient dynamo field had a dipolar morphology, a true polar wander is likely to have happened; the multipolar morphology is still a possibility; the dynamo field may vary very little in terms of its morphology.

5 Conclusion

Today the early history of Mercury is poorly constrained by in situ measurements. However, some constraints on the early history of Mercury might be found by analyzing its crustal magnetic field as measured by satellites. Magnetic anomalies that are generated by thermoremanently magnetized sources possess information on the ancient core field, and therefore it is important to distinguish them from sources generated by other magnetization processes. Here we study magnetic anomalies that are associated with complex craters on Mercury as their centered melt sheets are likely to be thermoremanently magnetized rather than shockremanently magnetized. During the crater formation, the iron rich impactor is incorporated mostly in the melt sheet that cools down slowly, recording thermoremanently the ambient magnetic field. However, as argued by (Hood et al., 2018), the amount of iron that an impactor can plausibly deliver to Mercury's surface falls well short of that needed to explain the observed relatively strong crater-associated magnetic anomalies as being induced in the present-day core dynamo field. Additionally, not all craters are associated with magnetic field anomalies as the composition of the impactor is expected to vary in iron content.

Here we use the crustal magnetic field model of (Hood, 2016) and (Hood et al., 2018) based on low magnetic field measurements of the MESSENGER spacecraft and estimate magnetization directions, which we then convert to magnetic paleopole positions. We employed the method of (Parker, 1991), which assumes a unidirectionally magnetized source. This is in agreement with a stable core-generated dipolar field present when the crater was formed. An important characteristic of this method is that it does not require

any assumptions on the source geometry. We studied five anomalies associated with craters suitable for inversion, and we obtained the corresponding magnetic paleopoles. Most of the best-fitting paleopoles are found at middle to high latitudes in the Southern Hemisphere although one is very close to the equator. Accounting for the uncertainties, which are calculated in a very conservative way, we find that our results converge towards a small region that excludes the current magnetic (and geographic South) pole.

No single physical process can satisfactorily explain the finding that our best fitting paleopoles are located in the southern hemisphere only, but away from the geographic pole. Assuming a dipolar field aligned with the rotation axis, true polar wander events from 27 up to 88 degrees are required. Reorientation models can only explain up to 20° of true polar wander when accounting for important masses added by impactors. Alternatively, their distribution might be also indicative of a different field morphology present at the surface of Mercury when the craters formed. However, it would be a major challenge for dynamo modelers to account for an abrupt change from a multipolar field to a very stable axisymmetric field morphology as observed by MESSENGER today. We found that the five anomalies solutions all agree in a smaller common solutions area that excludes the current geographic poles. This could be explained by a centered non-axial dipolar field, or by an axial dipolar field present before the planet has suffered a true polar wander.

Overall, our study strongly suggests that Mercury has evolved with time. Our results cannot decipher between changes caused by a true polar wander or evolution affecting the dynamo process. It should be emphasized that our study is limited by the small area of low altitude measurements containing crustal information due to MESSENGER's eccentric orbit. New results and conclusions may arise with BepiColombo ESA/JAXA mission (Benkhoff et al., 2010) launched in October 2018. The mission will return magnetic field measurements at low altitudes all around the planet. Hopefully, during this new mission or towards its end, other regions of Mercury's crustal magnetic field might be also measured and consequently increase our understanding of the early history of Mercury.

Acknowledgments

Maps used in this study are available at

$https://pds{-}ppi.igpp.ucla.edu/search/view/?f=yesid=pds://PPI/mess{-}mag-field-maps$.

We would like to thank the reviewers Foteini Vervelidou and Vincent Lesur for their valuable comments that helped to improve a first version of this manuscript. JSO is funded by the ESA Research Fellowship programme in Space Science. JSO and BL acknowledge the ANR project MARMITE (ANR-13-BS05-0012). This work was supported at the University of Arizona by the NASA DDAP. This study further benefited from the financial support from Région Pays de la Loire, project GeoPlaNet (convention 2016-10982).

References

Abrahams, J. N. H., Cao, H., & Stevenson, D. J. (2016, March). Inner Core Translation, True Polar Wander, and Mercury's North-South Asymmetric Magnetic Field. In *Proc. lunar planet. sci. conf.* (Vol. 47, p. Abstract 2502).

Anderson, B. J., Johnson, C. L., Korth, H., Winslow, R. M., Borovsky, J. E., Purucker, M. E., ... McNutt, R. L., Jr. (2012, December). Low-degree structure in Mercury's planetary magnetic field. *J. Geophys. Res.*, *117*, E00L12. doi: 10.1029/2012JE004159

Arkani-Hamed, J. (2001). Paleomagnetic pole positions and pole reversals of Mars. *Geophys. Res. Lett.*, *28*, 3409-3412. doi: 10.1029/2001GL012928

Benkhoff, J., van Casteren, J., Hayakawa, H., Fujimoto, M., Laakso, H., Novara, M., ... Ziethe, R. (2010). Bepicolombo—comprehensive exploration of mercury: Mission overview and science goals. *Planetary and Space Science*, *58*(1), 2 - 20. Retrieved from `http://www.sciencedirect.com/science/article/pii/S0032063309002840` (Comprehensive Science Investigations of Mercury: The scientific goals of the joint ESA/JAXA mission BepiColombo) doi: https://doi.org/10.1016/j.pss.2009.09.020

Bezaeva, N. S., Gattacceca, J., Rochette, P., Sadykov, R. A., & Trukhin, V. I. (2010, Mar). Demagnetization of terrestrial and extraterrestrial rocks under hydrostatic pressure up to 1.2 GPa. *Physics of the Earth and Planetary Interiors*, *179*(1-2), 7-20. doi: 10.1016/j.pepi.2010.01.004

Butler, R. (1992). *Paleomagnetism: Magnetic domains to geologic terranes*. Blackwell Scientific Publications. Retrieved from `https://books.google.co.in/books?id=q\_NzQgAACAAJ`

Cao, H., Aurnou, J. M., Wicht, J., Dietrich, W., Soderlund, K. M., & Russell, C. T. (2014). A dynamo explanation for mercury's anomalous magnetic field. *Geophys. Res. Lett.*, *41*. doi: 10.1002/2014GL060196

Christensen, U. R. (2006, December). A deep dynamo generating Mercury's magnetic field. *Nature*, *444*, 1056-1058. doi: 10.1038/nature05342

Christensen, U. R., & Wicht, J. (2008, July). Models of magnetic field generation in partly stable planetary cores: Applications to Mercury and Saturn. *Icarus*, *196*, 16-34. doi: 10.1016/j.icarus.2008.02.013

Cintala, M. J., & Grieve, R. A. F. (1998, July). Scaling impact-melt and crater dimensions: Implications for the lunar cratering record. *Meteorit. Planet. Sci.*, *33*, 889-912. doi: 10.1111/j.1945-5100.1998.tb01695.x

Gattacceca, J., Boustie, M., Lima, E., Weiss, B. P., de Resseguier, T., & Cuq-Lelandais, J. P. (2010, Sep). Unraveling the simultaneous shock magnetization and demagnetization of rocks. *Physics of the Earth and Planetary Interiors*, *182*(1-2), 42-49. doi: 10.1016/j.pepi.2010.06.009

Hauck II, S. A., Margot, J.-L., Solomon, S. C., Phillips, R. J., Johnson, C. L., Lemoine, F. G., ... Zuber, M. T. (2013). The curious case of mercury's internal structure. *Journal of Geophysical Research: Planets*, *118*(6), 1204-1220. Retrieved from `https://agupubs.onlinelibrary.wiley.com/doi/abs/10.1002/jgre.20091` doi: 10.1002/jgre.20091

Hood, L. L. (2015, December). Initial mapping of Mercury's crustal magnetic field: Relationship to the Caloris impact basin. *Geophys. Res. Lett.*, *42*, 10. doi: 10.1002/2015GL066451

Hood, L. L. (2016). Magnetic anomalies concentrated near and within mercury's impact basins: Early mapping and interpretation. *Journal of Geophysical Research: Planets*, *121*(6), 1016-1025. Retrieved from `https://agupubs.onlinelibrary.wiley.com/doi/abs/10.1002/2016JE005048` doi: 10.1002/2016JE005048

Hood, L. L., Oliveira, J. S., Galluzzi, V., & Rothery, D. A. (2018). Investigating sources of mercury's crustal magnetic field: Further mapping of messenger magnetometer data. *Journal of Geophysical Research: Planets*, *123*(10), 2647-2666. Retrieved from `https://agupubs.onlinelibrary.wiley.com/doi/abs/10.1029/2018JE005683` doi: 10.1029/2018JE005683

Johnson, C. L., Phillips, R. J., Purucker, M. E., Anderson, B. J., Byrne, P. K., Denevi, B. W., ... Solomon, S. C. (2015, May). Low-altitude magnetic field measurements by MESSENGER reveal Mercury's ancient crustal field. *Science*, *348*, 892-895. doi: 10.1126/science.aaa8720

Johnson, C. L., Purucker, M. E., Korth, H., Anderson, B. J., Winslow, R. M., Al Asad, M. M. H., ... Solomon, S. C. (2012, December). MESSENGER observations of Mercury's magnetic field structure. *J. Geophys. Res.*, *117*, E00L14. doi: 10.1029/2012JE004217

Katanforoush, A., & Shahshahani, M. (2003). Distributing Points on the Sphere. *Exper. Math.*, *12*, 199-209.

Keane, J. T., & Matsuyama, I. (2018, May). True Polar Wander of Mercury. In *Mercury: Current and future science of the innermost planet* (Vol. 2047, p. 6098).

Korth, H., Anderson, B. J., Johnson, C. L., Winslow, R. M., Slavin, J. A., Purucker, M. E., ... McNutt, R. L., Jr. (2012, December). Characteristics of the plasma distribution in Mercury's equatorial magnetosphere derived from MESSENGER Magnetometer observations. *Journal of Geophysical Research (Space Physics)*, *117*, A00M07. doi: 10.1029/2012JA018052

Lawson, C. L., & Hanson, R. J. (1974). *Solving least squares problems.* Englewood Cliffs, NJ 07632, USA: Prentice-Hall.

Le Bars, M., Wieczorek, M. A., Karatekin, Ö., Cébron, D., & Laneuville, M. (2011, November). An impact-driven dynamo for the early Moon. *Nature*, *479*, 215-218. doi: 10.1038/nature10565

Matsuyama, I., Nimmo, F., & Mitrovica, J. X. (2014). Planetary reorientation. *Annual Review of Earth and Planetary Sciences*, *42*(1), 605-634. Retrieved from `https://doi.org/10.1146/annurev-earth-060313-054724` doi: 10.1146/annurev-earth-060313-054724

Oliveira, J. S., Langlais, B., Pais, M. A., & Amit, H. (2015). A modified equivalent source dipole method to model partially distributed magnetic field measurements, with application to Mercury. *Journal of Geophysical Research: Planets*, *120*(6), 1075-1094. Retrieved from `https://agupubs.onlinelibrary.wiley.com/doi/abs/10.1002/2014JE004734` doi: 10.1002/2014JE004734

Oliveira, J. S., & Wieczorek, M. A. (2017, February). Testing the axial dipole hy-

pothesis for the Moon by modeling the direction of crustal magnetization. *J. Geophys. Res. Planets*, *122*, 383-399. doi: 10.1002/2016JE005199

Oliveira, J. S., Wieczorek, M. A., & Kletetschka, G. (2017). Iron abundances in lunar impact basin melt sheets from orbital magnetic field data. *Journal of Geophysical Research: Planets*, *122*(12), 2429-2444. Retrieved from `https://agupubs.onlinelibrary.wiley.com/doi/abs/10.1002/2017JE005397` doi: 10.1002/2017JE005397

Parker, R. L. (1991, September). A Theory of Ideal Bodies for Seamount Magnetism. *J. Geophys. Res.*, *96*, 16101-16112. doi: 10.1029/91JB01497

Purucker, M. E., Sabaka, T. J., Solomon, S. C., Anderson, B. J., Korth, H., Zuber, M. T., & Neumann, G. A. (2009). Mercury's internal magnetic field: Constraints on large- and small-scale fields of crustal origin. *Earth and Planetary Science Letters*, *285*(3), 340 - 346. Retrieved from `http://www.sciencedirect.com/science/article/pii/S0012821X08007681` (MESSENGER's First Flyby of Mercury) doi: https://doi.org/10.1016/j.epsl.2008.12.017

Stanley, S., Bloxham, J., Hutchison, W. E., & Zuber, M. T. (2005). Thin shell dynamo models consistent with mercury's weak observed magnetic field. *Earth and Planetary Science Letters*, *234*(1), 27 - 38. Retrieved from `http://www.sciencedirect.com/science/article/pii/S0012821X05001652` doi: https://doi.org/10.1016/j.epsl.2005.02.040

Strauss, B. E., Feinberg, J. M., & Johnson, C. L. (2016). Magnetic mineralogy of the mercurian lithosphere. *Journal of Geophysical Research: Planets*, *121*(11), 2225-2238. Retrieved from `https://agupubs.onlinelibrary.wiley.com/doi/abs/10.1002/2016JE005054` doi: 10.1002/2016JE005054

Tagle, R., & Hecht, L. (2006, November). Geochemical identification of projectiles in impact rocks. *Meteorit. Planet. Sci.*, *41*, 1721-1735. doi: 10.1111/j.1945-5100.2006.tb00448.x

Tagle, R., Schmitt, R. T., & Erzinger, J. (2009, August). Identification of the projectile component in the impact structures Rochechouart, France and Sääksjärvi, Finland: Implications for the impactor population for the earth. *Geochim. Cosmochim. Ac.*, *73*, 4891-4906. doi: 10.1016/j.gca.2009.05.044

Takahashi, F., & Matsushima, M. (2006). Dipolar and non-dipolar dynamos

in a thin shell geometry with implications for the magnetic field of mercury. *Geophysical Research Letters*, *33*(10). Retrieved from https://agupubs.onlinelibrary.wiley.com/doi/abs/10.1029/2006GL025792 doi: 10.1029/2006GL025792

Takahashi, F., Shimizu, H., & Tsunakawa, H. (2019). Mercury's anomalous magnetic field caused by a symmetry-breaking self-regulating dynamo. *Nature Communications*, *10*(1), 208. Retrieved from https://doi.org/10.1038/s41467-018-08213-7 doi: 10.1038/s41467-018-08213-7

Takahashi, F., Tsunakawa, H., Shimizu, H., Shibuya, H., & Matsushima, M. (2014, June). Reorientation of the early lunar pole. *Nature Geosci.*, *7*, 409-412. doi: 10.1038/ngeo2150

Thébault, E., Langlais, B., Oliveira, J. S., Amit, H., & Leclercq, L. (2018). A time-averaged regional model of the hermean magnetic field. *Physics of the Earth and Planetary Interiors*, *276*, 93 - 105. Retrieved from http://www.sciencedirect.com/science/article/pii/S0031920117300304 (Special Issue:15th SEDI conference) doi: https://doi.org/10.1016/j.pepi.2017.07.001

Thomas, P., Grott, M., Morschhauser, A., & Vervelidou, F. (2018). Paleopole reconstruction of martian magnetic field anomalies. *Journal of Geophysical Research: Planets*, *123*(5), 1140-1155. Retrieved from https://agupubs.onlinelibrary.wiley.com/doi/abs/10.1002/2017JE005511 doi: 10.1002/2017JE005511

Vervelidou, F., & Lesur, V. (2018). Unveiling earth's hidden magnetization. *Geophysical Research Letters*, *45*(22), 12,283-12,292. Retrieved from https://agupubs.onlinelibrary.wiley.com/doi/abs/10.1029/2018GL079876 doi: 10.1029/2018GL079876

Vervelidou, F., Lesur, V., Morschhauser, A., Grott, M., & Thomas, P. (2017, December). On the accuracy of palaeopole estimations from magnetic field measurements. *Geophysical Journal International*, *211*, 1669-1678. doi: 10.1093/gji/ggx400

Vilim, R., Stanley, S., & Hauck, S. A. (2010, November). Iron snow zones as a mechanism for generating Mercury's weak observed magnetic field. *J. Geophy. Res. (Planets)*, *115*, 11003. doi: 10.1029/2009JE003528

Vine, F. J., & Matthews, D. H. (1963, September). Magnetic Anomalies Over

Oceanic Ridges. *Nature*, *199*, 947-949. doi: 10.1038/199947a0

Weider, S. Z., Nittler, L. R., Starr, R. D., McCoy, T. J., & Solomon, S. C. (2014). Variations in the abundance of iron on mercury's surface from messenger x-ray spectrometer observations. *Icarus*, *235*, 170 - 186. Retrieved from http://www.sciencedirect.com/science/article/pii/S0019103514001195 doi: https://doi.org/10.1016/j.icarus.2014.03.002

Wieczorek, M. A., Weiss, B. P., & Stewart, S. T. (2012, March). An impactor origin for lunar magnetic anomalies. *Science*, *335*, 1212. doi: 10.1126/science.1214773

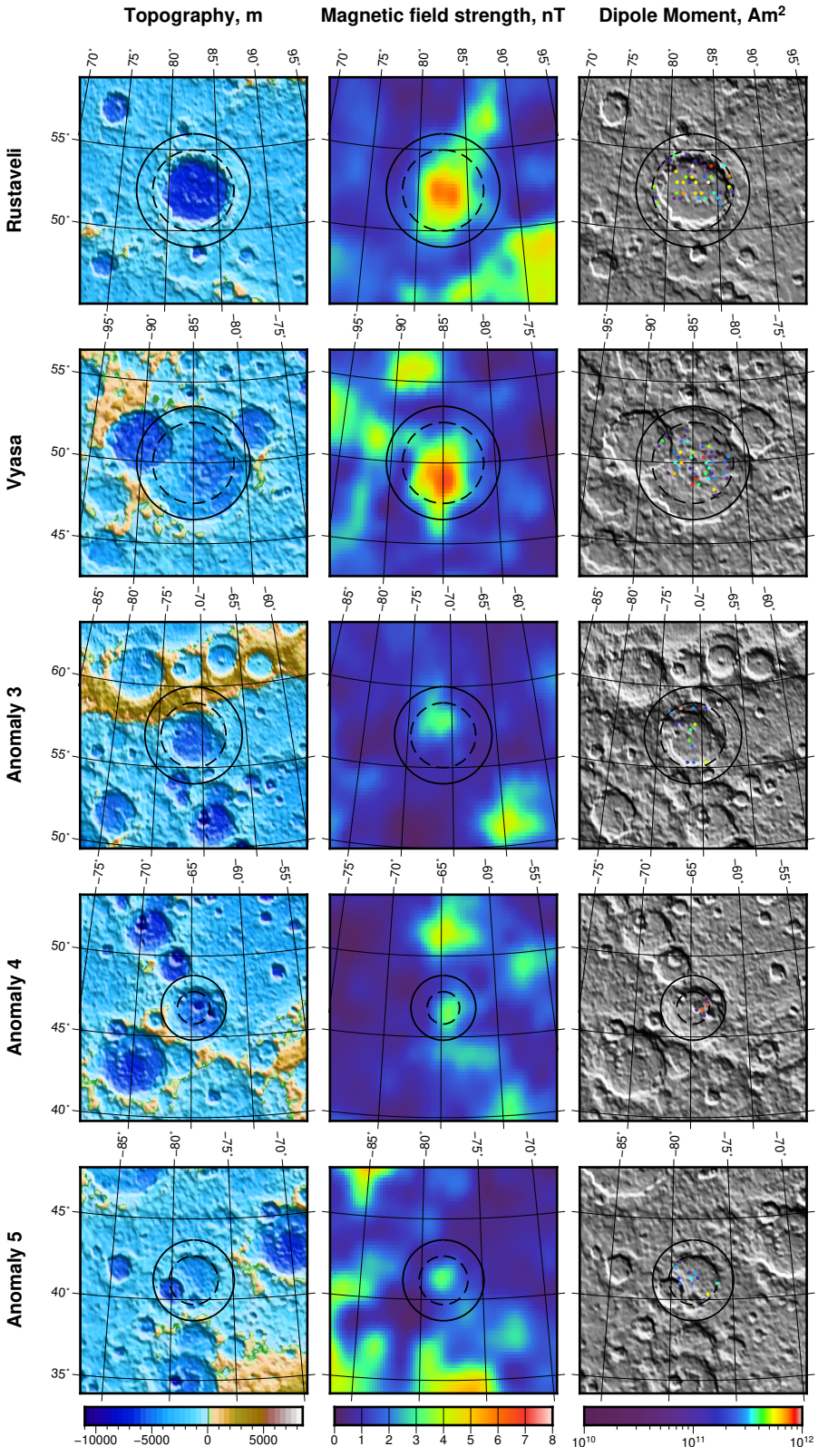

Figure 2. Modeling summary for each of the five crater-associated anomalies: Left column: topography; middle column: observed magnetic field strength at 40 km altitude; right column: magnetic moments of the retained dipoles used in the inversions. Also shown in the supporting information is the radial magnetic field data component, the best fitting radial magnetic field (i.e., the modelled field), and the difference between the two. Black circles delimit the grid of observations (solid line) and dipoles (dashed line). Images are presented using a Lambert azimuthal equal-area projection.

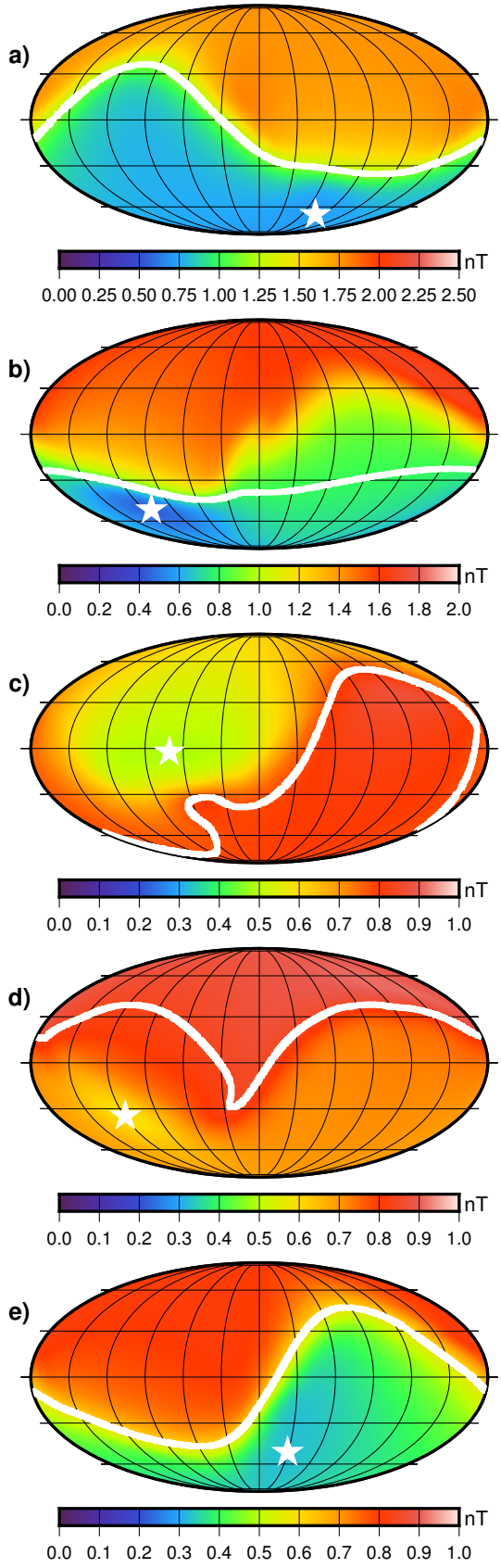

Figure 3. Misfit as a function of north paleomagnetic pole position with the corresponding uncertainty denoted by a white solid line for Rustaveli (a), Vyasa (b), anomaly 3 (c), anomaly 4 (d), and anomaly 5 (e). The star denotes the best fitting solution. Results are presented using a global Molleweide projection with a central meridian of 0°.

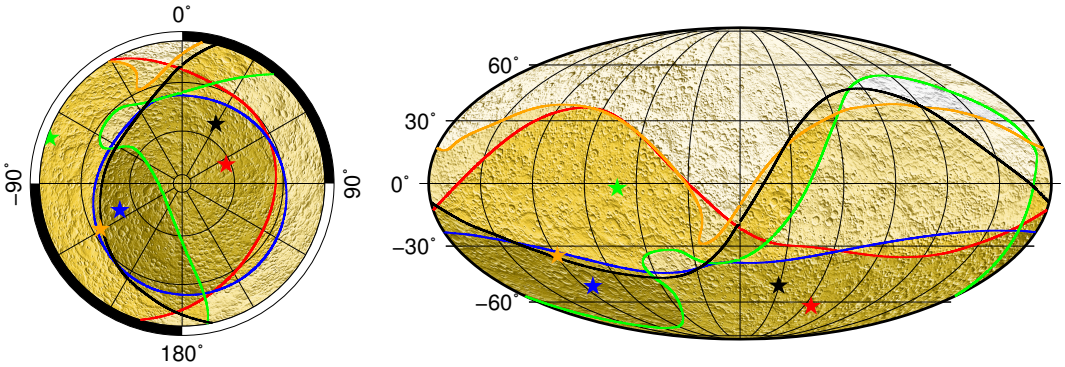

Figure 4. North paleomagnetic pole positions for all studied crustal magnetic anomalies: (red) Rustaveli, (blue) Vyasa, (green) Anomaly3, (orange) Anomaly 4 and, (black) Anomaly5. The maps are: (left) in a Lambert Azimuthal Equal Area projection with the south pole in the center and, (right) in a Molleweide projection centered at 0°E. The darker yellow color corresponds to regions with a higher probability of containing the solution.

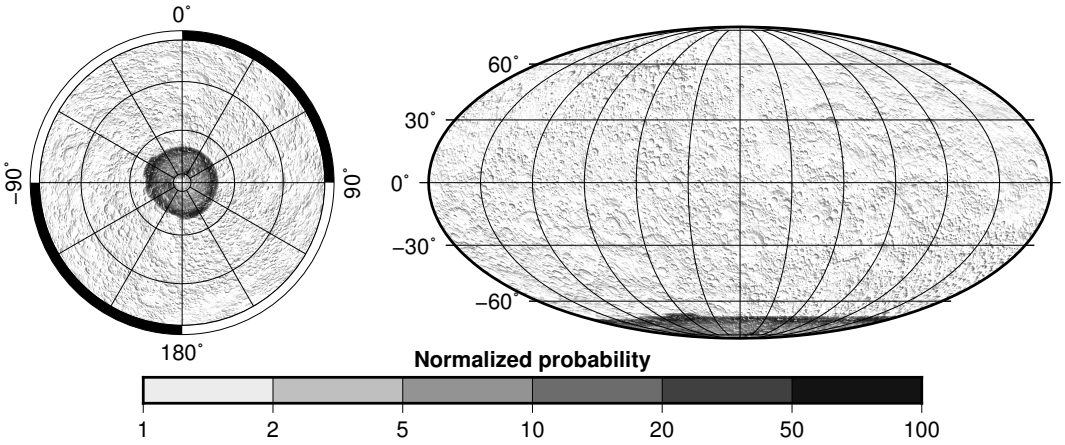

Figure 5. Distribution of paleopoles under the assumption of a dipolar field using a present day core field model for Mercury. The maps are: (left) in a Lambert Azimuthal Equal Area projection with the south pole in the center and, (right) in a Molleweide projection centered at 0°E. The maximum normalized probability corresponds to 40%.

Figure 1.

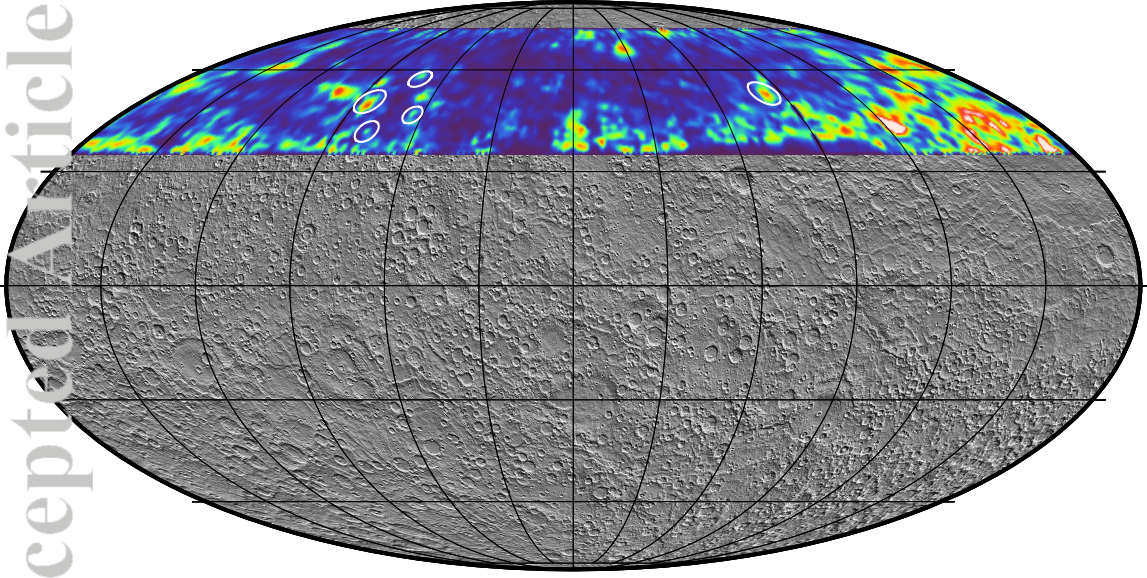

Figure 2.

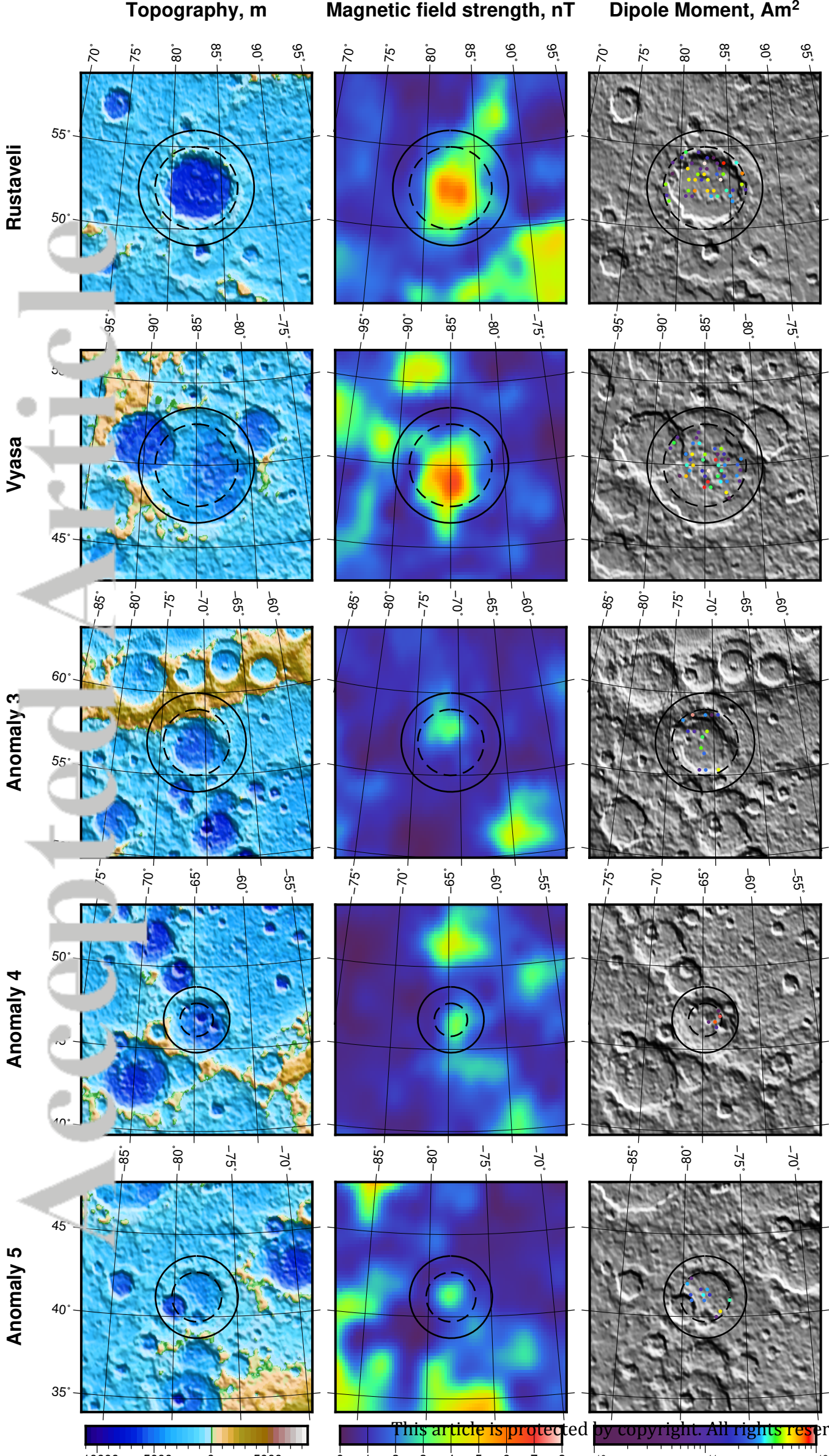

Figure 3.

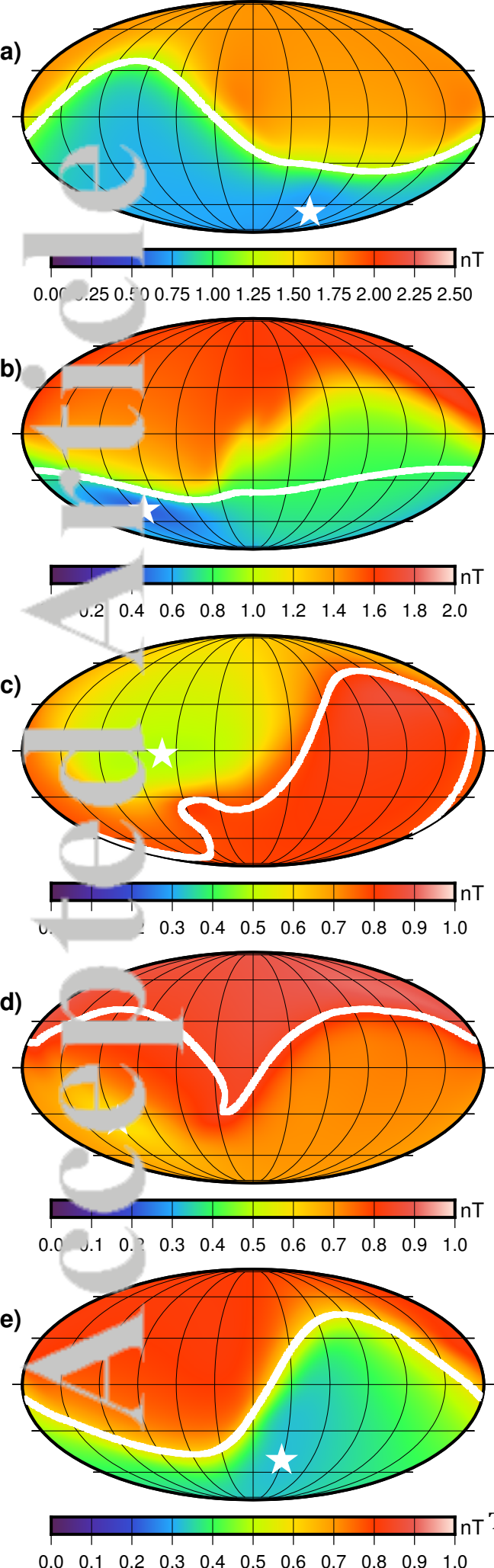

Figure 4.

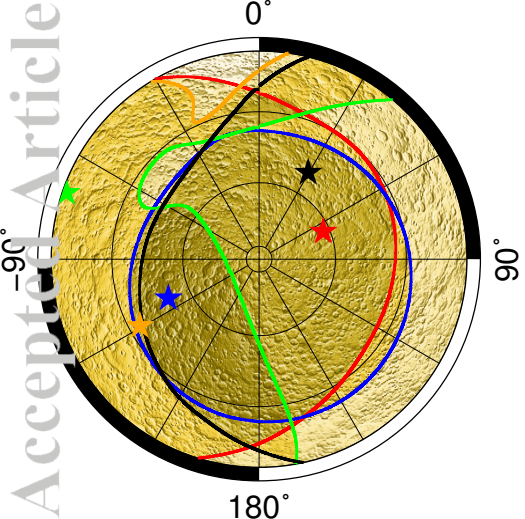

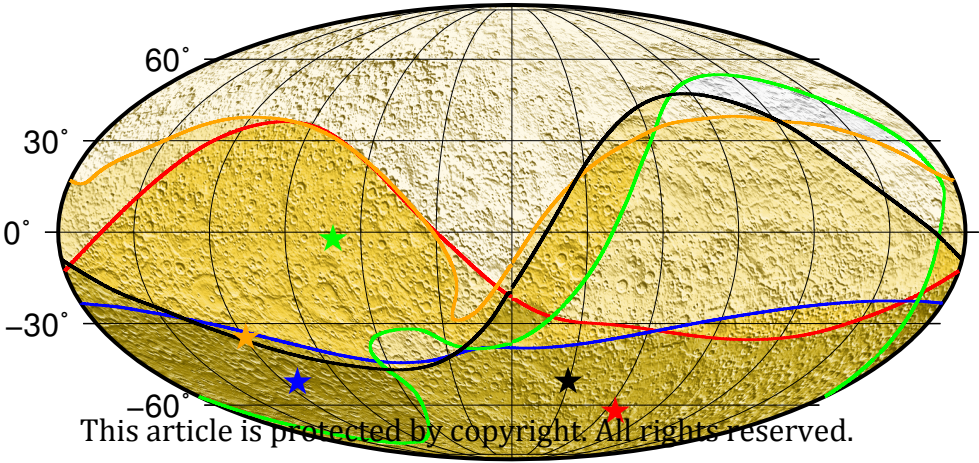

Figure 5.